

Karatsuba Matrix Multiplication and its Efficient Custom Hardware Implementations

Trevor E. Pogue  and Nicola Nicolici , *Senior Member, IEEE*

Abstract—While the Karatsuba algorithm reduces the complexity of large integer multiplication, the extra additions required minimize its benefits for smaller integers of more commonly-used bitwidths. In this work, we propose the extension of the scalar Karatsuba multiplication algorithm to matrix multiplication, showing how this maintains the reduction in multiplication complexity of the original Karatsuba algorithm while reducing the complexity of the extra additions. Furthermore, we propose new matrix multiplication hardware architectures for efficiently exploiting this extension of the Karatsuba algorithm in custom hardware. We show that the proposed algorithm and hardware architectures can provide real area or execution time improvements for integer matrix multiplication compared to scalar Karatsuba or conventional matrix multiplication algorithms, while also supporting implementation through proven systolic array and conventional multiplier architectures at the core. We provide a complexity analysis of the algorithm and architectures and evaluate the proposed designs both in isolation and in an end-to-end deep learning accelerator system compared to baseline designs and prior state-of-the-art works implemented on the same type of compute platform, demonstrating their ability to increase the performance-per-area of matrix multiplication hardware.

Index Terms—Hardware architecture, systolic arrays, performance, throughput, Karatsuba, machine learning

I. INTRODUCTION

THE demand for optimized hardware acceleration of general matrix multiplication (GEMM) continues to drive innovation in the field of hardware design for exploiting the inherent parallelism to speed up computation. At a certain point, however, after the known parallelism and system-level optimizations are exhausted and technology scaling slows to a halt, there is an accelerator wall which limits further progress on the implementation side [1]. A less-explored direction for continuing advancement beyond this wall is through reducing the workload at the algebraic level, by computing the same result from a re-arranged compute pattern requiring fewer or cheaper operations to be performed in hardware.

Multiply-accumulate (MAC) units are commonly the area-dominant computational resource in GEMM and deep learning accelerators [2], [3], [4], and due to this, an accelerator’s throughput can be directly limited by how many multipliers its hardware budget can afford. As a result, surpassing this performance per multiplier limit has been focused on recently with minimal filtering algorithms applied to convolutional neural networks [2], [5], as well fast inner-product algorithms for GEMM and machine learning workloads [6]. Along this same

direction, the Karatsuba algorithm [7] can also theoretically be used to reduce the complexity of integer multiplication. However, the extra addition operations it introduces can increase its execution speed in general-purpose computers or limit its area reduction in custom multiplier circuits for smaller integers of more commonly-used bitwidths [8], [9].

In this work, we show how the scalar Karatsuba multiplication algorithm can be extended to integer matrix multiplication, after which the impact and complexity of the extra additions is reduced. Furthermore, we investigate and present new fixed-precision and precision-scalable hardware architectures for efficiently exploiting the Karatsuba algorithm extended to matrix multiplication (referred to as Karatsuba matrix multiplication or KMM), showing how the proposed algorithm and hardware architectures can provide real area or execution time reductions for integer matrix multiplication compared to scalar Karatsuba or conventional matrix multiplication.

The proposed architectures can also be implemented using proven systolic array and conventional multiplier architectures at their core, maintaining all the implementation benefits of these architectures. Systolic arrays, which we will also refer to as matrix multiplication units (MXU)s for convenience, are an effective choice for use in GEMM accelerators as they significantly reduce the required memory traffic and can reach high clock frequencies due to their short and regular interconnects. Systolic-array architectures have been used in state-of-the-art GEMM and deep learning accelerators such as the Tensor Processing Unit (TPU) [3], [4], [10], among others [6], [11].

In summary, our key contributions are the following:

- We propose the Karatsuba matrix multiplication (KMM) algorithm and carry out a complexity analysis of the algorithm compared to conventional scalar Karatsuba and matrix multiplication algorithms to facilitate further future investigations of potential applications and hardware implementations of KMM. We also identify complexity shortcomings of KMM that restrict its benefits in hardware and show how this is mitigated when KMM is combined with an alternative accumulation algorithm.
- We present a new family of hardware architectures for efficiently exploiting KMM in custom hardware. We then model the area or execution time benefits of the KMM architectures and evaluate the proposed architectures both in isolation and in an end-to-end accelerator system compared to baseline designs and prior state-of-the-art works implemented on the same type of compute platform.

T. E. Pogue and N. Nicolici are with the Department of Electrical and Computer Engineering, McMaster University, Hamilton, ON, L8S 4L8, Canada
Email: poguete@mcmaster.ca; nicolici@mcmaster.ca

Conventional 2-Digit Scalar Multiplication (SM₂)

$$\begin{aligned}
 & a \times b \\
 &= (a_1 \ll w/2 + a_0) \times (b_1 \ll w/2 + b_0) \\
 &= \begin{array}{cccc} a_1 & a_0 & a_1 & a_0 \\ \otimes & \otimes & \otimes & \otimes \\ b_1 & b_1 & b_0 & b_0 \\ \downarrow & \downarrow & \downarrow & \downarrow \\ a_1 b_1 \ll w & + & a_1 b_0 \ll w/2 & + \\ & & a_0 b_1 \ll w/2 & + \\ & & & a_0 b_0 \end{array}
 \end{aligned}$$

Fig. 1. SM₂ algorithm illustration.

II. BACKGROUND AND RELATED WORK

A. Notation

We use the following notation throughout this article:

- ALG_{*n*}^[*w*]: An algorithm that operates on *w*-bit scalars or matrices with *w*-bit elements, where each scalar or matrix element is divided into *n* digits. For example, SM₂^[8] represents a scalar multiplication (SM) algorithm for operating on 8-bit 2-digit numbers where each digit is 4 bits wide, such as the multiplication between the hexadecimal values 0x12 × 0x10 = 0x120.
- ALG_{*n*} or ALG: The algorithm acronym may also be specified without the subscript *n* and/or superscript [*w*] when the number of digits and/or input bitwidths are not directly relevant for the current context, and it may refer to the use of the algorithm for any value of *n* or *w* for each missing subscript and/or superscript.
- OPERATION^[*w*]: An arithmetic operation that works with *w*-bit values. For example, MULT^[*w*], ADD^[*w*], ACCUM^[*w*] represent a multiplication, addition, and accumulation of *w*-bit values, respectively, and SHIFT^[*w*] represents a left or right shift by *w* bits.
- x^[*a*:*b*]: The value contained in bits *a* down to *b* of a scalar *x*. For example, the value of bits 7 down to 4 in the hexadecimal number 0xAE is equal to 0xA and is written as 0xAE^[7:4] = 0xA. Similarly, 0xAE^[3:0] = 0xE.
- C(ALG_{*n*}^[*w*]): The complexity of algorithm ALG in number of *w*-bit multiplications, additions, accumulations, and shift operations.
- C(ALG_{*n*}): The complexity of algorithm ALG in number of arithmetic operations.
- *r*: The number of recursion levels implemented in KSM or KMM, equal to ⌈log₂*n*⌉.
- *d*: The height and width of two matrices being multiplied.

B. Conventional *n*-Digit Scalar Multiplication (SM)

Fig. 1 shows the conventional method for performing 2-digit scalar multiplication where a *w*-bit multiplication is split into four smaller-bit scalar multiplications before being summed to form the final product. Algorithm 1 shows the generalization of this, where *n*-digit multiplication is performed by carrying out the same steps recursively for each smaller-bit multiplication.

Algorithm 1 Conventional *n*-Digit Scalar Multiplication.

```

1: function SMn[w](a, b)
2:   if (n > 1) then
3:     a1 = a[w-1:⌈w/2⌉]
4:     a0 = a[⌈w/2⌉-1:0]
5:     b1 = b[w-1:⌈w/2⌉]
6:     b0 = b[⌈w/2⌉-1:0]
7:     c1 = SMn/2[⌈w/2⌉](a1, b1)
8:     c10 = SMn/2[⌈w/2⌉](a1, b0)
9:     c01 = SMn/2[⌈w/2⌉](a0, b1)
10:    c0 = SMn/2[⌈w/2⌉](a0, b0)
11:    c = c1 ⌊⌊ w
12:    c += (c01 + c10) ⌊⌊ ⌈w/2⌉
13:    c += c0
14:  else
15:    c = a × b
16:  end if
17:  return c
18: end function

```

2-Digit Karatsuba Scalar Multiplication (KSM₂)

$$\begin{aligned}
 & a \times b \\
 &= (a_1 \ll w/2 + a_0) \times (b_1 \ll w/2 + b_0) \\
 &= \begin{array}{ccc} a_1 & (a_1 + a_0) & a_0 \\ \otimes & \otimes & \otimes \\ b_1 & (b_1 + b_0) & b_0 \\ \downarrow & \downarrow & \downarrow \\ a_1 b_1 \ll w & + & (a_1 b_0 + a_0 b_1) \ll w/2 + a_0 b_0 \\ & & \begin{array}{l} + a_1 b_0 \\ + a_0 b_1 \\ - a_0 b_0 \\ - a_1 b_1 \end{array} \end{array}
 \end{aligned}$$

Fig. 2. KSM₂ algorithm illustration. Compared to SM₂, KSM₂ requires only 3 single-digit multiplications, however, it requires 3 more additions, increasing the overall operation count.

C. Karatsuba Scalar Multiplication (KSM)

Fig. 2 shows the Karatsuba algorithm [7] for 2-digit scalar multiplication where a *w*-bit multiplication is split this time into *three* smaller-bit multiplications before being summed to form the final product. Algorithm 2 shows the generalization of this, where *n*-digit multiplication is performed by carrying out the same steps recursively for each smaller-bit multiplication.

KSM-based low-bitwidth accurate integer multiplier circuits in prior works have shown some area benefits for input bitwidths in the range of 64 bits or less, with minimal area improvements in the smallest ranges of 16 bits [8], [9].

D. Conventional *n*-Digit Matrix Multiplication (MM)

A conventional matrix multiplication algorithm computes $\mathbf{C} = \mathbf{AB}$ for \mathbf{A} of size $M \times K$ and \mathbf{B} of size $K \times N$, where each element $c_{i,j}$ of \mathbf{C} is calculated as follows:

$$c_{i,j} = \sum_{k=1}^K a_{i,k} b_{k,j}. \quad (1)$$

Algorithm 2 n-Digit Karatsuba Scalar Multiplication.

```

1: function  $\text{KSM}_n^{[w]}(a, b)$ 
2:   if ( $n > 1$ ) then
3:      $a_1 = a^{[w-1:[w/2]}$ 
4:      $a_0 = a^{[[w/2]-1:0]}$ 
5:      $b_1 = b^{[w-1:[w/2]}$ 
6:      $b_0 = b^{[[w/2]-1:0]}$ 
7:      $a_s = a_1 + a_0$ 
8:      $b_s = b_1 + b_0$ 
9:      $c_1 = \text{KSM}_{n/2}^{[[w/2]]}(a_1, b_1)$ 
10:     $c_s = \text{KSM}_{n/2}^{[[w/2]+1]}(a_s, b_s)$ 
11:     $c_0 = \text{KSM}_{n/2}^{[[w/2]]}(a_0, b_0)$ 
12:     $c = c_1 \ll w$ 
13:     $c += (c_s - c_1 - c_0) \ll [w/2]$ 
14:     $c += c_0$ 
15:  else
16:     $c = a \times b$ 
17:  end if
18:  return  $c$ 
19: end function

```

Conventional 2-Digit Matrix Multiplication (MM_2)

$$\begin{aligned}
& \begin{bmatrix} \mathbf{A} \\ \mathbf{B} \end{bmatrix} \times \begin{bmatrix} \mathbf{B} \\ \mathbf{B} \end{bmatrix} \\
&= \left(\begin{bmatrix} \mathbf{A}_1 \\ \mathbf{A}_0 \end{bmatrix} \ll w/2 + \begin{bmatrix} \mathbf{A}_0 \\ \mathbf{A}_0 \end{bmatrix} \right) \times \left(\begin{bmatrix} \mathbf{B}_1 \\ \mathbf{B}_0 \end{bmatrix} \ll w/2 + \begin{bmatrix} \mathbf{B}_0 \\ \mathbf{B}_0 \end{bmatrix} \right) \\
&= \begin{bmatrix} \mathbf{A}_1 \\ \mathbf{A}_0 \end{bmatrix} \otimes \begin{bmatrix} \mathbf{B}_1 \\ \mathbf{B}_0 \end{bmatrix} + \begin{bmatrix} \mathbf{A}_1 \\ \mathbf{A}_0 \end{bmatrix} \otimes \begin{bmatrix} \mathbf{B}_0 \\ \mathbf{B}_0 \end{bmatrix} + \begin{bmatrix} \mathbf{A}_0 \\ \mathbf{A}_0 \end{bmatrix} \otimes \begin{bmatrix} \mathbf{B}_1 \\ \mathbf{B}_0 \end{bmatrix} + \begin{bmatrix} \mathbf{A}_0 \\ \mathbf{A}_0 \end{bmatrix} \otimes \begin{bmatrix} \mathbf{B}_0 \\ \mathbf{B}_0 \end{bmatrix} \\
&= \begin{bmatrix} \mathbf{A}_1 \mathbf{B}_1 \\ \mathbf{A}_1 \mathbf{B}_0 \\ \mathbf{A}_0 \mathbf{B}_1 \\ \mathbf{A}_0 \mathbf{B}_0 \end{bmatrix} \ll w/2 + \begin{bmatrix} \mathbf{A}_1 \mathbf{B}_0 \\ \mathbf{A}_0 \mathbf{B}_0 \end{bmatrix}
\end{aligned}$$

Fig. 3. MM_2 algorithm illustration. The 4 single-digit matrix multiplications of complexity $\mathcal{O}(d^3)$ dominate the $\mathcal{O}(d^2)$ complexity of the matrix additions.

The method in Fig. 1 can also be extended to matrix multiplication as illustrated in Fig. 3, where four separate partial-product matrix multiplications are performed between matrices each containing bit slices of every element, and they are later summed together to form the final matrix product. Algorithm 3 shows the generalization of this, where n-digit matrix multiplication is performed by carrying out the same steps recursively for each smaller-bit matrix multiplication. The elements in matrices \mathbf{A}_0 and \mathbf{B}_0 contain the lower bits (bits $[w/2] - 1$ down to 0) of every element in the \mathbf{A} and \mathbf{B} matrices, while \mathbf{A}_1 and \mathbf{B}_1 contain the upper bits (bits $w - 1$ down to $[w/2]$) of every element in matrices \mathbf{A} and \mathbf{B} . This allows for w -bit matrix multiplication using smaller m -bit multipliers. The MM_1 algorithm on line 15 of Algorithm 3 is a conventional matrix multiplication algorithm such as (1).

E. Precision-Scalable Architectures

Precision-scalable architectures allow a way to efficiently execute workloads across multiple input precisions for applications where the input bitwidths are expected to vary. Machine learning (ML) acceleration is one example of a use-case for precision-scalable hardware architectures, where neural networks can perform the majority of the inference on

Algorithm 3 Conventional n-Digit Matrix Multiplication.

```

1: function  $\text{MM}_n^{[w]}(\mathbf{A}, \mathbf{B})$ 
2:   if ( $n > 1$ ) then
3:      $\mathbf{A}_1 = \begin{bmatrix} a_{1,1}^{[w-1:[w/2]}, & \dots & a_{1,K}^{[w-1:[w/2]} \\ \dots & \dots & \dots \\ a_{M,1}^{[w-1:[w/2]}, & \dots & a_{M,K}^{[w-1:[w/2]} \\ a_{1,1}^{[[w/2]-1:0]}, & \dots & a_{1,K}^{[[w/2]-1:0]} \end{bmatrix}$ 
4:      $\mathbf{A}_0 = \begin{bmatrix} a_{1,1}^{[[w/2]-1:0]}, & \dots & a_{1,K}^{[[w/2]-1:0]} \\ \dots & \dots & \dots \\ a_{M,1}^{[[w/2]-1:0]}, & \dots & a_{M,K}^{[[w/2]-1:0]} \\ b_{1,1}^{[w-1:[w/2]}, & \dots & b_{1,N}^{[w-1:[w/2]} \end{bmatrix}$ 
5:      $\mathbf{B}_1 = \begin{bmatrix} b_{1,1}^{[w-1:[w/2]}, & \dots & b_{1,N}^{[w-1:[w/2]} \\ \dots & \dots & \dots \\ b_{K,1}^{[w-1:[w/2]}, & \dots & b_{K,N}^{[w-1:[w/2]} \\ b_{1,1}^{[[w/2]-1:0]}, & \dots & b_{1,N}^{[[w/2]-1:0]} \end{bmatrix}$ 
6:      $\mathbf{B}_0 = \begin{bmatrix} b_{1,1}^{[[w/2]-1:0]}, & \dots & b_{1,N}^{[[w/2]-1:0]} \\ \dots & \dots & \dots \\ b_{K,1}^{[[w/2]-1:0]}, & \dots & b_{K,N}^{[[w/2]-1:0]} \end{bmatrix}$ 
7:      $\mathbf{C}_1 = \text{MM}_{n/2}^{[[w/2]]}(\mathbf{A}_1, \mathbf{B}_1)$ 
8:      $\mathbf{C}_{10} = \text{MM}_{n/2}^{[[w/2]]}(\mathbf{A}_1, \mathbf{B}_0)$ 
9:      $\mathbf{C}_{01} = \text{MM}_{n/2}^{[[w/2]]}(\mathbf{A}_0, \mathbf{B}_1)$ 
10:     $\mathbf{C}_0 = \text{MM}_{n/2}^{[[w/2]]}(\mathbf{A}_0, \mathbf{B}_0)$ 
11:     $\mathbf{C} = \mathbf{C}_1 \ll w$ 
12:     $\mathbf{C} += (\mathbf{C}_{10} + \mathbf{C}_{01}) \ll [w/2]$ 
13:     $\mathbf{C} += \mathbf{C}_0$ 
14:  else
15:     $\mathbf{C} = \text{MM}_1^{[w]}(\mathbf{A}, \mathbf{B})$ 
16:  end if
17:  return  $\mathbf{C}$ 
18: end function

```

reduced-bitwidth operations with little to no loss in accuracy but the bitwidths required to provide sufficient accuracy vary across different deep neural network models, applications, and between individual layers within the same neural network model [12]. For example, some neural network models can be executed with high accuracy even when performing the majority of the operations on small bitwidths, however, a smaller portion of the layers still need to be computed on larger bitwidths to preserve accuracy [12]. Therefore, a fixed-bitwidth accelerator must make a trade-off between either supporting only lower bitwidths while reducing the model's accuracy, or supporting larger bitwidths for higher accuracy but under-utilizing the MAC units during majority of computation as most stages require only lower-bit inputs.

Precision-scalable architectures address this trade-off by providing architectures which can more efficiently support execution of varying input bitwidths [12], [13], [14]. One approach is to use MAC units consisting of multiple smaller-bitwidth multipliers [13] which can either be individually used to multiply/accumulate multiple smaller-bitwidth products, or they can be reconfigured to collectively multiply/accumulate fewer larger-bitwidth products per clock cycle. Another type of approach referred to as bit-serial architectures [14], is to have MAC arrays which repeatedly perform fixed-size smaller-bitwidth vector operations on different bit slices of the vectors, summing up the separate vector products to get the final full-bitwidth vector result.

The hardware algorithms used in prior works on precision-scalable architectures [12], [13], [14] use variations of the

$$\begin{aligned}
& \text{2-Digit Karatsuba Matrix Multiplication (KMM}_2\text{)} \\
& = \frac{(\mathbf{A}_1 \ll w/2 + \mathbf{A}_0) \times (\mathbf{B}_1 \ll w/2 + \mathbf{B}_0)}{} \\
& \begin{array}{c}
\mathbf{A}_1 \xrightarrow{\mathcal{O}(d^2)} (\mathbf{A}_1 + \mathbf{A}_0) \xrightarrow{\mathcal{O}(d^3)} \mathbf{A}_0 \\
\mathbf{B}_1 \xrightarrow{\mathcal{O}(d^2)} (\mathbf{B}_1 + \mathbf{B}_0) \xrightarrow{\mathcal{O}(d^3)} \mathbf{B}_0 \\
\mathbf{A}_1 \mathbf{B}_1 \ll w + \left(\begin{array}{l} \mathbf{A}_1 \mathbf{B}_0 \\ \mathbf{A}_0 \mathbf{B}_1 \\ \mathbf{A}_0 \mathbf{B}_0 \end{array} \right) \ll w/2 + \mathbf{A}_0 \mathbf{B}_0 \\
\phantom{\mathbf{A}_1 \mathbf{B}_1 \ll w +} \left(\begin{array}{l} \mathbf{A}_1 \mathbf{B}_0 \\ \mathbf{A}_0 \mathbf{B}_1 \end{array} \right) \ll w/2 + \mathbf{A}_0 \mathbf{B}_0 \\
\phantom{\mathbf{A}_1 \mathbf{B}_1 \ll w +} - \left(\begin{array}{l} \mathbf{A}_0 \mathbf{B}_0 \\ \mathbf{A}_1 \mathbf{B}_1 \end{array} \right)
\end{array}
\end{aligned}$$

Fig. 4. KMM₂ algorithm illustration. Compared to the scalar algorithms KSM₂ versus SM₂, the increase in number of additions with complexity $\mathcal{O}(d^2)$ in KMM₂ versus MM₂ is now insignificant relative to the reduction of 3 instead of 4 single-digit matrix multiplications of complexity $\mathcal{O}(d^3)$, allowing the overall #operations in KMM₂ to be less than conventional MM₂.

SM and MM algorithms shown in Algorithms 1 and 3 to combine partial products and compute variable-bitwidth w -bit matrix products using smaller m -bit multipliers, where the number of m -bit multiplications and minimum possible execution time if fully utilizing the m -bit multipliers scales quadratically with the input bitwidths w . However, as shown later, the minimum possible execution time of a precision-scalable KMM architecture scales less than quadratically with the input bitwidths w .

III. KARATSUBA MATRIX MULTIPLICATION (KMM)

In this section, we formally define KMM, analyze its complexity compared to conventional scalar Karatsuba and matrix multiplication algorithms, identify complexity shortcomings of the KMM algorithm that restrict its benefits in hardware, and show how this is mitigated when combining KMM with an alternative accumulation algorithm.

A. KMM Definition

Fig. 4 shows the 2-digit Karatsuba scalar multiplication algorithm [7] from Fig. 2 extended to matrix multiplication analogously to how Fig. 3 extends conventional 2-digit scalar multiplication in Fig. 1 to matrix multiplication. Algorithm 4 shows the generalization of this, where n -digit Karatsuba matrix multiplication is performed by carrying out the same steps recursively for each smaller-bit matrix multiplication. In Algorithm 4, the full matrix product is split into three separate partial-product matrix multiplications between matrices each containing bit slices of every element. The elements in matrices \mathbf{A}_0 and \mathbf{B}_0 contain the lower bits (bits $\lceil w/2 \rceil - 1$ down to 0) of every element in the \mathbf{A} and \mathbf{B} matrices, while \mathbf{A}_1 and \mathbf{B}_1 contain the upper bits (bits $w-1$ down to $\lceil w/2 \rceil$) of every element in matrices \mathbf{A} and \mathbf{B} . The \mathbf{A}_s and \mathbf{B}_s matrices are formed by summing $\mathbf{A}_1 + \mathbf{A}_0$ and $\mathbf{B}_1 + \mathbf{B}_0$, and

Algorithm 4 n -Digit Karatsuba Matrix Multiplication.

```

1: function KMMn[w](A, B)
2:   if (n > 1) then
3:     A1 =  $\begin{bmatrix} a_{1,1}^{[w-1:\lceil w/2 \rceil]} & \dots & a_{1,K}^{[w-1:\lceil w/2 \rceil]} \\ \dots & \dots & \dots \\ a_{M,1}^{[w-1:\lceil w/2 \rceil]} & \dots & a_{M,K}^{[w-1:\lceil w/2 \rceil]} \end{bmatrix}$ 
4:     A0 =  $\begin{bmatrix} a_{1,1}^{[\lceil w/2 \rceil-1:0]} & \dots & a_{1,K}^{[\lceil w/2 \rceil-1:0]} \\ \dots & \dots & \dots \\ a_{M,1}^{[\lceil w/2 \rceil-1:0]} & \dots & a_{M,K}^{[\lceil w/2 \rceil-1:0]} \end{bmatrix}$ 
5:     B1 =  $\begin{bmatrix} b_{1,1}^{[w-1:\lceil w/2 \rceil]} & \dots & b_{1,N}^{[w-1:\lceil w/2 \rceil]} \\ \dots & \dots & \dots \\ b_{K,1}^{[w-1:\lceil w/2 \rceil]} & \dots & b_{K,N}^{[w-1:\lceil w/2 \rceil]} \end{bmatrix}$ 
6:     B0 =  $\begin{bmatrix} b_{1,1}^{[\lceil w/2 \rceil-1:0]} & \dots & b_{1,N}^{[\lceil w/2 \rceil-1:0]} \\ \dots & \dots & \dots \\ b_{K,1}^{[\lceil w/2 \rceil-1:0]} & \dots & b_{K,N}^{[\lceil w/2 \rceil-1:0]} \end{bmatrix}$ 
7:     As = A1 + A0
8:     Bs = B1 + B0
9:     C1 = KMMn/2[ $\lceil w/2 \rceil$ ](A1, B1)
10:    Cs = KMMn/2[ $\lceil w/2 \rceil + 1$ ](As, Bs)
11:    C0 = KMMn/2[ $\lceil w/2 \rceil$ ](A0, B0)
12:    C = C1  $\ll$  w
13:    C += (Cs - C1 - C0)  $\ll$   $\lceil w/2 \rceil$ 
14:    C += C0
15:   else
16:     C = MM1[w](A, B)
17:   end if
18:   return C
19: end function

```

therefore their elements have a bitwidth of $\lceil w/2 \rceil + 1$. The partial-product matrices are then summed analogously to how the partial scalar products are summed after multiplication in KSM from Algorithm 2.

B. KMM Complexity Analysis

In this subsection, we derive the complexity of KMM and compare it to the complexity of the conventional MM, and KSM algorithms. To do this, we decompose each algorithms' complexity to number of w -bit multiplications, additions, and shift operations. This provides a general technology-agnostic foundation for evaluating different possible KMM hardware implementations and modelling the costs and benefits of implementing the algorithm in hardware across different possible implementation technologies where the cost of each type of operation may vary depending on the implementation platform used. For example, implementations on FPGA may result in multipliers mapping to DSP units, additions and accumulations mapping to soft look-up-table (LUT) and register resources, whereas ASIC implementations will result in different costs and trade-offs than this for each type of operation.

Additionally, while the main focus of this work is on leveraging KMM in custom hardware designs, we also compare KMM's complexity more simply in number of arithmetic operations to allow modelling the time complexity of KMM execution on general-purpose hardware containing fixed operator word sizes. This analysis (plotted in Fig. 5) indicates that KMM requires significantly fewer operations to execute large-integer matrix multiplication on general-purpose hardware

than conventional KSM or MM algorithms. This is relevant when the matrix element bitwidths are larger than the word size of the general-purpose hardware operators, for example, inputs larger than 32 bits when executing on a CPU containing arithmetic logic units (ALUs) that support 32-bit inputs.

1) *MM Complexity*: The complexity of conventional n -digit MM between two matrices of size $d \times d$ is derived by counting the number of operations that are performed in Algorithm 3:

$$\begin{aligned} C(\text{MM}_n^{[w]}) &= C(\text{MM}_{n/2}^{\lfloor w/2 \rfloor}) + 3C(\text{MM}_{n/2}^{\lceil w/2 \rceil}) \\ &\quad + d^2 \left(\text{ADD}^{[w+w_a]} + 2\text{ADD}^{[2w+w_a]} \right) \\ &\quad + d^2 \left(\text{SHIFT}^{[w]} + \text{SHIFT}^{\lceil w/2 \rceil} \right) \end{aligned} \quad (2a)$$

$$C(\text{MM}_1^{[w]}) = d^3 \left(\text{MULT}^{[w]} + \text{ACCUM}^{[2w]} \right). \quad (2b)$$

Typically, $\text{ACCUM}^{[2w]} = \text{ADD}^{[2w+w_a]}$, where w_a is an additional bitwidth added to account for accumulation. However, in Section III-C, we discuss a method for reducing the complexity of the accumulations to be less than this.

The $\text{ADD}^{[w+w_a]}$ terms in (2a) come from the additions forming the $(\mathbf{C}_{10} + \mathbf{C}_{01})$ term on line 12 of Algorithm 3. Here, the bitwidth of the \mathbf{C}_{10} and \mathbf{C}_{01} elements is $w + w_a$ because they are accumulations of w -bit products of $\lfloor w/2 \rfloor$ and $\lceil w/2 \rceil$ -bit values. The two $\text{ADD}^{[2w+w_a]}$ terms in (2a) come from the additions to \mathbf{C} on lines 12 and 13 of Algorithm 3. The bitwidth of these additions is kept on $2w + w_a$ bits since \mathbf{C} results in accumulations of $2w$ -bit products of w -bit values.

2) *KSM Complexity*: The complexity of KSM is derived by counting the operations performed in Algorithm 2:

$$\begin{aligned} C(\text{KSM}_n^{[w]}) &= 2 \left(\text{ADD}^{[2w]} + \text{ADD}^{\lceil w/2 \rceil} + \text{ADD}^{[2\lceil w/2 \rceil+4]} \right) \\ &\quad + \text{SHIFT}^{[w]} + \text{SHIFT}^{\lceil w/2 \rceil} \\ &\quad + C(\text{KSM}_{n/2}^{\lfloor w/2 \rfloor}) + C(\text{KSM}_{n/2}^{\lceil w/2 \rceil+1}) \\ &\quad + C(\text{KSM}_{n/2}^{\lceil w/2 \rceil}) \end{aligned} \quad (3a)$$

$$C(\text{KSM}_1^{[w]}) = \text{MULT}^{[w]}. \quad (3b)$$

The two $\text{ADD}^{\lceil w/2 \rceil}$ terms in (3a) come from the $\lceil w/2 \rceil$ -bit additions forming the a_s and b_s terms on lines 7 and 8 of Algorithm 2. The two $\text{ADD}^{[2\lceil w/2 \rceil+4]}$ terms in (3a) come from forming the $(c_s - c_1 - c_0)$ term on line 13 of Algorithm 2, where these terms can be first summed together on $2\lceil w/2 \rceil + 4$ bits before being shifted and added to the other product terms. The bitwidth $2\lceil w/2 \rceil + 4$ is required because c_s is a $(2\lceil w/2 \rceil + 2)$ -bit product of $(\lceil w/2 \rceil + 1)$ -bit values, and the additional two bits are to account for sign extension and subtraction of the c_1 and c_0 terms. The two $\text{ADD}^{[2w]}$ terms in (3a) come from the additions to c on lines 13 and 14 of Algorithm 2. These additions are on $2w$ -bit values since c will ultimately result in the $2w$ -bit product of two w -bit values.

3) *KSMM Complexity*: To compare KSM to KMM and the other matrix multiplication algorithms, we analyze the complexity of an algorithm we refer to as KSMM. KSMM is defined as a conventional matrix multiplication algorithm as in (1), but where KSM is used for the multiplications between all elements rather than conventional scalar multiplication.

KSMM then has the following complexity:

$$C(\text{KSMM}_n^{[w]}) = d^3 \left(C(\text{KSM}_n^{[w]}) + \text{ACCUM}^{[2w]} \right). \quad (4)$$

4) *KMM Complexity*: The complexity of KMM is derived by counting the operations performed in Algorithm 4:

$$\begin{aligned} C(\text{KMM}_n^{[w]}) &= 2d^2 \left(\text{ADD}^{[2\lceil w/2 \rceil+4+w_a]} + \text{ADD}^{[2w+w_a]} \right) \\ &\quad + d^2 \left(2\text{ADD}^{\lceil w/2 \rceil} + \text{SHIFT}^{[w]} + \text{SHIFT}^{\lceil w/2 \rceil} \right) \\ &\quad + C(\text{KMM}_{n/2}^{\lfloor w/2 \rfloor}) + C(\text{KMM}_{n/2}^{\lceil w/2 \rceil+1}) \\ &\quad + C(\text{KMM}_{n/2}^{\lceil w/2 \rceil}) \end{aligned} \quad (5a)$$

$$C(\text{KMM}_1^{[w]}) = C(\text{MM}_1^{[w]}). \quad (5b)$$

The two $\text{ADD}^{\lceil w/2 \rceil}$ terms in (5a) come from the $\lceil w/2 \rceil$ -bit additions forming the \mathbf{A}_s and \mathbf{B}_s terms on lines 7 and 8 of Algorithm 4. The two $\text{ADD}^{[2\lceil w/2 \rceil+4+w_a]}$ terms in (5a) come from forming the $(\mathbf{C}_s - \mathbf{C}_1 - \mathbf{C}_0)$ term on line 13 of Algorithm 4, where these terms can be first summed together on $2\lceil w/2 \rceil + 4 + w_a$ bits before being shifted and added to the other product terms. The bitwidth $2\lceil w/2 \rceil + 4 + w_a$ is required because the bitwidth of \mathbf{C}_s is $2\lceil w/2 \rceil + 2 + w_a$ since it is accumulations of $(2\lceil w/2 \rceil + 2)$ -bit products of $(\lceil w/2 \rceil + 1)$ -bit values, and the additional two bits are to account for sign extension and subtraction of the \mathbf{C}_1 and \mathbf{C}_0 terms. The two $\text{ADD}^{[2w+w_a]}$ terms in (5a) come from the additions to \mathbf{C} on lines 13 and 14 of Algorithm 4. The bitwidth of these additions is kept on $2w + w_a$ bits since \mathbf{C} results in accumulations of $2w$ -bit products of w -bit values.

(5a) shows that KMM significantly reduces the complexity of the 8 addition and shift operations in (3a) that are performed $(n/2)^{\log_2 3} d^3$ times in KSMM by reducing their occurrence by a factor of d . On the other hand, KMM trades d^3 accumulations of $2w$ -bit values in (2b) or (4) for $n^{\log_2 3} d^3$ smaller-width accumulations in (5b). However, in Section III-C we show how the penalty of this in hardware is mitigated when combining KMM with an alternative accumulation algorithm.

5) *Arithmetic complexity*: If only counting the number of operations without considering operation bitwidths or type, we can simplify (2) to:

$$C(\text{MM}_n) = 2n^2 d^3 + 5(n/2)^2 d^2, \quad (6)$$

(4) can be simplified to:

$$C(\text{KSMM}_n) = (1 + 11(n/2)^{\log_2 3}) d^3, \quad (7)$$

and (5) can be simplified to:

$$C(\text{KMM}_n) = (n/2)^{\log_2 3} (6d^3 + 8d^2). \quad (8)$$

C. Mitigating the Accumulator Complexity Increase in KMM

As found in Section III-B, KMM has one penalty of trading d^3 accumulations of $2w$ -bit values in (2b) or (4) for $n^{\log_2 3} d^3$ smaller-width accumulations in (5b). In this subsection, we show how this downside is mitigated when using Algorithm 5 as the MM_1 algorithm in KMM on line 16 of Algorithm 4. Algorithm 5 performs MM_1 using an alternative accumulation structure that reduces the accumulation hardware complexity.

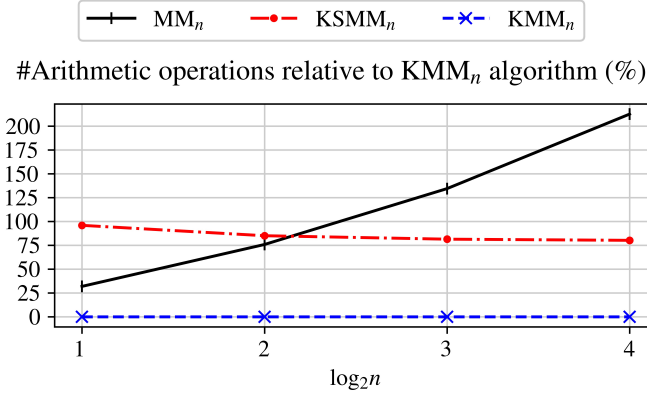


Fig. 5. Plotting (6) and (7) relative to (8) for different n with $d = 64$. As can be seen, $KSMM_n$ requires over 75% more operations than KMM_n . Additionally, KMM_n and $KSMM_n$ require exponentially fewer operations than MM_n with respect to n , however, KMM_n requires fewer operations than MM_n even starting at $n = 2$, while $KSMM_n$ does not fall below MM_n until $n > 4$.

Algorithm 5 MM_1 algorithm with reduced accumulator complexity used in the baseline MM_1 MXUs of all compared architectures. p is defined as the number of multiplication products that are pre-accumulated on a smaller bitwidth to reduce the accumulation complexity before being added to the full-bitwidth accumulation sum. We use $p = 4$ in our evaluation.

```

1: function  $MM_1(A, B, p)$ 
2:   for  $i = 0; i < M; i ++$  do
3:     for  $j = 0; j < N; j ++$  do
4:        $C_{i,j} = 0$ 
5:       for  $k = 0; k < K; k += p$  do
6:          $x = 0$ 
7:         for  $q = 0; q < p; q ++$  do
8:            $x += A_{i,k+q} \times B_{k+q,j}$ 
9:         end for
10:         $C_{i,j} += x$ 
11:      end for
12:    end for
13:  end for
14:  return C
15: end function

```

In conventional matrix multiplication, each product of w -bit elements is added to a running sum kept on $2w + w_a$ bits, where $w_a = \lceil \log_2 d \rceil$ and is an extra bitwidth added to account for accumulation in order to accumulate d elements which adds extra hardware complexity. This means that normally p accumulations of $2w$ -bit elements will require being added to a $(2w + w_a)$ -bit running sum and each addition will be on $2w + w_a$ bits and therefore contain the following complexity:

$$p \text{ ACCUM}^{[2w]} = p \text{ ADD}^{[2w+w_a]}. \quad (9)$$

However, the average bitwidth of the addition operations is reduced when using Algorithm 5 for accumulation of p elements of bitwidth $2w$ because p elements are first added together in isolation on a smaller running sum requiring a bitwidth of only $2w + w_p$ bits for keeping p elements, where $w_p = \lceil \log_2 p \rceil$. Only after this initial pre-sum will this result then be added to the full running sum that is kept on a larger

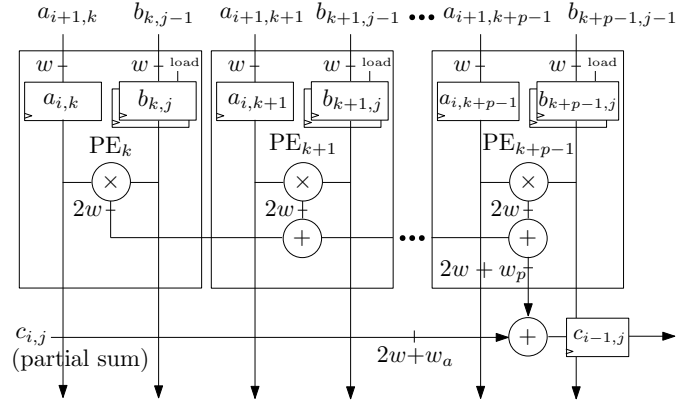


Fig. 6. Showing the internal PE structure of the MM_1 MXUs shown in Fig. 7 as well as the structure for implementing Algorithm 5 in hardware to reduce the hardware cost of the accumulator logic. p is a hardware parameter equal to the number of multiplication products that are pre-accumulated on a smaller bitwidth to reduce the accumulation complexity before being added to the full-bitwidth accumulation sum. We use $p = 4$ in our evaluation.

$2w + w_a$ bits for keeping d elements. This reduces the average bitwidth for every p accumulations to the following:

$$p \text{ ACCUM}^{[2w]} = \text{ADD}^{[2w+w_a]} + (p - 1) \text{ ADD}^{[2w+w_p]}. \quad (10)$$

Furthermore, in systolic-array architectures, each accumulation output is buffered in a dedicated register, which adds further hardware complexity to the accumulation operation. However, the number of required accumulation registers when using Algorithm 5 is also reduced by a factor of p as shown in the hardware implementation from Fig. 6 in Sections IV-A since the accumulation result only needs to be buffered after being added to the full running sum kept on $2w + w_a$ bits.

IV. KMM HARDWARE ARCHITECTURES

In this section, we present a general family of hardware architectures for efficiently exploiting the KMM algorithm in hardware and derive metrics for analyzing the area or execution time benefits of the KMM architectures. The first type of KMM architecture, described in Section IV-B, is a fixed-precision architecture optimized for executing inputs that are not expected to vary in bitwidth. We then present a precision-scalable KMM architecture in Section IV-C that can more efficiently execute across multiple input precisions for applications where the input bitwidths are expected to vary.

A. Baseline MM_1 Architecture

Fig. 7 shows the internal structure of each baseline MM_1 MXU at the core of each KMM architecture, and Fig. 6 shows the internal structure of the processing elements (PE)s inside the MM_1 MXUs. Fig. 6 also shows the structure for how Algorithm 5 from Section III-C can be implemented in hardware and how the algorithm is able to reduce the hardware cost of the accumulator logic. This accumulation structure allows for the number of $(2w + w_a)$ -bit accumulation adders and their output registers to be reduced by a factor of p , where they are instead traded for additions on lower-bitwidth values in the range of $2w$ to $2w + \lceil \log_2 p \rceil$ bits that do not require their output to be buffered in registers.

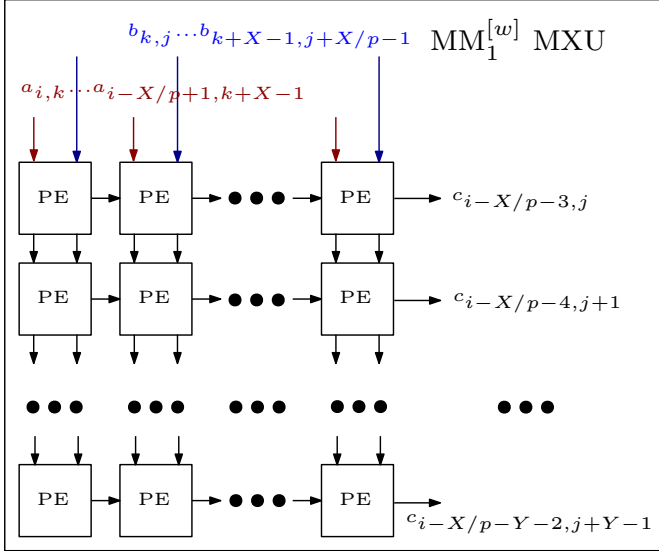


Fig. 7. Baseline MM_1 MXU architecture present at the core of the KMM architectures, provided for context. X and Y refer to the MXU width and height in number of multipliers.

B. Fixed-Precision KMM Architecture

Fig. 8 shows the proposed fixed-precision KMM architecture for executing on inputs of a fixed precision of w bits that are not expected to vary in bitwidth. Rather than having one MXU with w -bit-input multiplier units, this architecture consists of three sub-MXUs that compute matrix multiplication on either $\lfloor w/2 \rfloor$, $\lfloor w/2 \rfloor + 1$, or $\lceil w/2 \rceil$ -bit inputs.

The additions on lines 7 and 8 of Algorithm 4 are performed on X scalar adders at the MXU inputs. Similarly, the additions on lines 13 and 14 of Algorithm 4 are performed on Y scalar adders at the MXU outputs. Due to the nature of right/left shifting by a constant offset in custom hardware, the shift operations at the output of the MXUs do not require any area overhead. If desired, each of the three sub-MXUs can also be instantiated as another KMM MXU containing three more sub-MXUs to implement additional levels of KMM recursion. The final level of MXUs will be MM_1 MXUs.

C. Precision-Scalable KMM Architecture

Fig. 10 shows the proposed precision-scalable KMM architecture for implementing one level of KMM recursion. This architecture can more efficiently use m -bit-input multipliers to execute across varying input precisions of bitwidth w for applications where the input bitwidths are expected to vary. Unlike in prior works [12], [13], [14], the minimum possible execution time when fully utilizing the compute resources scales less than quadratically with the input bitwidths. As discussed further in Section IV-D, the input matrices are divided into tiles and fed into the MXU one-by-one to perform GEMM. In this architecture, each set of input matrix tiles may be read multiple times and either the MM_1 , MM_2 , or KMM_2 algorithm may be executed depending on the input bitwidths w and the multiplier bitwidth m . An iteration state signal t is reset when a new set of input tiles is read and is incremented each time the same set of input tiles is re-read.

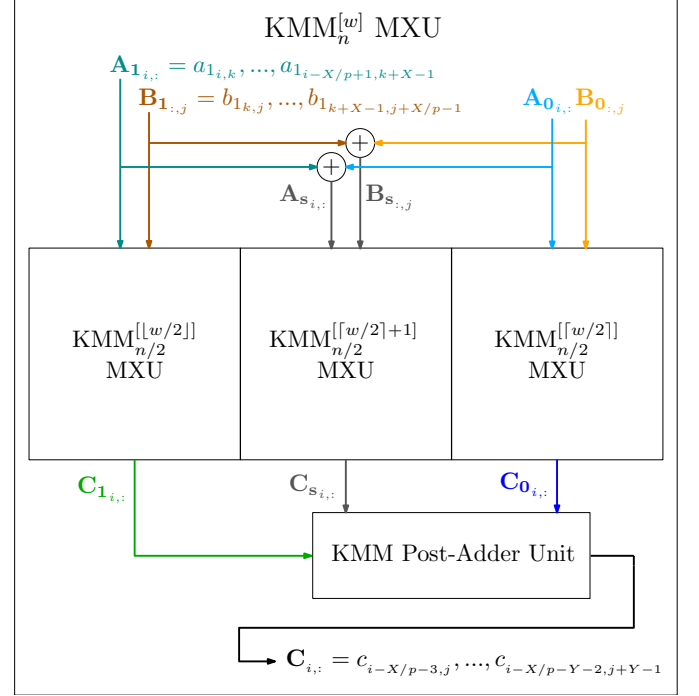


Fig. 8. Fixed-precision KMM architecture for executing on inputs of a fixed precision of w bits.

KMM Post-Adder Unit

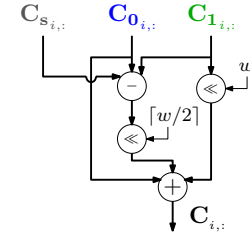


Fig. 9. KMM Post-Adder Unit from Fig. 8 for executing $C_{1_{i,:}} \ll w + (C_{s_{i,:}} - C_{1_{i,:}} - C_{0_{i,:}}) \ll \lfloor w/2 \rfloor + C_{0_{i,:}}$.

1) MM_1 and MM_2 Mode: If $w \leq m$, the architecture will execute the MM_1 algorithm, bypassing any MXU input/output addition or shifting steps, A_0 and B_0 will be fed into the MXU as inputs, and each set of input tiles is read only once.

If $2m - 2 < w \leq 2m$, the architecture will execute the MM_2 algorithm and each set of input matrix tiles will be read a total of four times before proceeding to the next set of input tiles. The MM_2 algorithm is used instead of KMM_2 for this input bitwidth range because the bitwidth of the elements in the A_s and B_s matrices in Algorithm 4 would be too large by 1 bit to fit onto the m -bit multipliers in the MXU. In each read for this input bitwidth range, the MXU will accept either the A_1 and B_1 inputs or the A_0 and B_0 inputs depending on the tile read iteration t . A_1 and B_1 will contain bits $2m - 1$ down to m of the A and B matrix elements. A_0 and B_0 will contain bits $m - 1$ down to 0 of the A and B matrix elements.

The MXU output vectors $C_{x_{i,:}}$ in Fig. 10 will be equal to either $(C_{1_{i,:}} \ll 2m)$, $(C_{10_{i,:}} \ll m)$, $(C_{01_{i,:}} \ll m)$, or

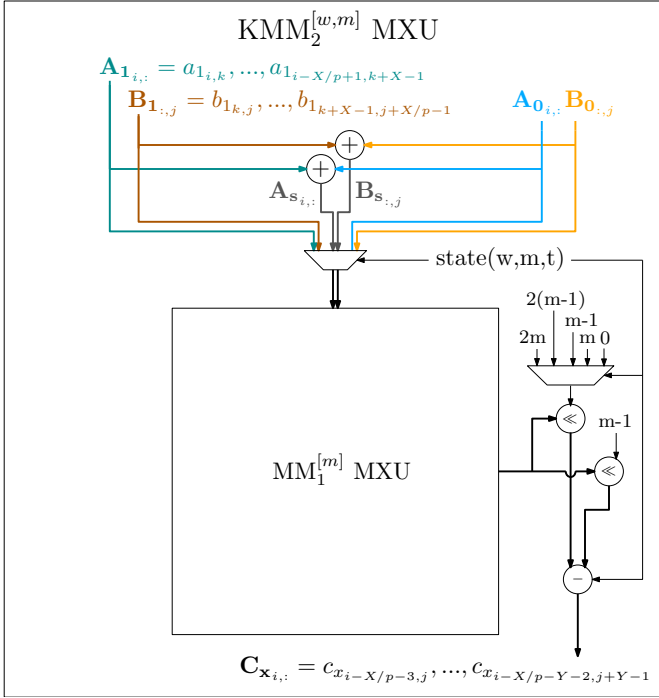


Fig. 10. Precision-scalable KMM architecture for more efficiently using m -bit-input multipliers to execute across varying input precisions of bitwidth w for applications where the input bitwidths are expected to vary.

$C_{0,i,:}$ depending on the tile read iteration t to incrementally execute lines 11-13 of Algorithm 3 throughout the tile read iterations, where m is considered equivalent to the value of $\lceil w/2 \rceil$ in Algorithm 3. Specifically, depending on the tile read iteration t , the MXU output vectors will be equal to $(C_{1,i,:} \ll 2m)$ to form the addition on line 11 of Algorithm 3, $C_{0,i,:}$ to form the addition on line 13, and separately $(C_{10,i,:} \ll m)$ or $(C_{01,i,:} \ll m)$ to collectively form the addition on line 12.

Each partial matrix tile product will need to be accumulated with prior ones outside of the MXU, however, this is the same functionality already present in GEMM where multiple matrix tile products must be summed to form a final matrix product, and this functionality will therefore already be present in GEMM and ML accelerator system from our prior work [6].

2) *KMM₂ Mode*: If $m < w \leq 2m - 2$, the architecture will execute the KMM₂ algorithm and each set of input matrix tiles will be read a total of three times before proceeding to the next set of input tiles. For each read, the MXU will accept or form either the A_1 and B_1 inputs, the A_s and B_s inputs, or the A_0 and B_0 inputs depending on the tile read iteration t . A_1 and B_1 will contain bits $2(m-1) - 1$ down to $m-1$ of the A and B matrix elements. A_0 and B_0 will contain bits $m-2$ down to 0 of the A and B matrix elements. The MXU output vectors $C_{x,i,:}$ in Fig. 10 will be equal to either $[(C_{1,i,:} \ll 2(m-1)) - (C_{1,i,:} \ll (m-1))]$, $[C_{s,i,:} \ll (m-1)]$, or $[C_{0,i,:} - (C_{0,i,:} \ll (m-1))]$ depending on the tile read iteration t to incrementally execute lines 12-14 of Algorithm 4 throughout the tile read iterations, where $m-1$ is considered equivalent to the value of $\lceil w/2 \rceil$ in Algorithm 4.

Each partial matrix tile product will need to be accumulated with prior ones outside of the MXU, however, this functionality will already be present in GEMM accelerators as explained above in Section IV-C1.

A precision-scalable MM₂ architecture can also be implemented that has a similar structure as the precision-scalable KMM architecture, except that it will only either execute the MM₁ algorithm if $w \leq m$ or the MM₂ algorithm if $m < w \leq 2m$. We also note that a precision-scalable KSMM architecture exploiting KSM₂ would not be as efficient to implement in hardware compared to a precision-scalable KMM architecture. This is because, in addition to the extra adders that would be required at the output/inputs of every multiplier as discussed in Section III-B, multiplexers would also have to be placed at the output/inputs of every multiplier in the MXU as well for output/input arbitration depending on the width of the inputs. In contrast, the KMM architecture reduces this extra adder complexity as already discussed, and it can employ an efficient more conventional systolic array at the core not requiring multiplexers surrounding each multiplier.

D. System Integration

In order to perform GEMM on an MXU and multiply matrices of arbitrary sizes that can be larger than the MXU dimensions, the input matrices are divided into tiles and fed to the MXU one-by-one. Following each tile multiplication, the partial tile products are accumulated outside of the MXU to generate each final matrix product tile. Prior to each tile multiplication, a B tile is loaded into the MXU. It then remains in place as the A tile flows through the MXU producing the tile product, during which a new $A_{i,:}$ vector is fed into the MXU each clock cycle. Additionally, to hide the latency of loading B tiles, the MXU PEs each contain one extra b buffer to load the next B tile into the MXU as the current tile is being multiplied, where each extra b buffer in the PEs will hold one individual element of the next B tile after it is loaded.

The presented KMM architectures are illustrated for unsigned integer inputs, however, if the inputs are signed, a 1-dimensional adder vector can be used to add a constant offset to the inputs of an MXU to convert them to unsigned. The zero-point adjuster method from our previous work [6] can then be used to efficiently eliminate the effects of this constant offset in the matrix products before exiting the MXU.

We use an ML accelerator system design based on the one from our previous work [6], which has open-source code available [15], to house and evaluate the KMM and baseline MXU architectures. We were able to swap the precision-scalable KMM MXU architecture from Fig. 8 into our system design [6] in place of the free-pipeline fast inner-product (FFIP) MXU. This change was mostly seamless but also required updates to the memory system such that each set of input matrix tiles can optionally be re-read up to three or four times before proceeding to the next set of input tiles. The number of times that the matrix tiles are re-read and the purpose for this is explained in Section IV-C.

E. Multiplier Compute Efficiency

In this subsection, we define a performance-per-area metric called the multiplier compute efficiency in (12) which we use to compare the KMM architecture against baseline designs and prior works. The metric is used to compare the amount of computational work that can be performed per compute area regardless of the clock frequency or input bitwidths. The importance of this property is expanded upon more later in this subsection, as well as in Section V-A.

The hardware complexity of fixed-point multipliers typically scale quadratically with the input bitwidth compared to linearly for adders and registers [16], [17], [18], causing the hardware footprint of multipliers to dominate that of adders and registers. Due to this, multipliers and MAC units are commonly the area-dominant computational resources in deep learning and GEMM-based accelerators [2], [3], [4]. Therefore, we derive a performance-per-area metric defined below for quantifying how much the algebraic optimizations exploited in an architecture reduce the computational complexity of the area-dominant operations (multiplications) and measure how effectively an architecture can utilize these resources relative to a conventional design using no algebraic optimizations:

$$\frac{\text{mults/multiplier}}{\text{clock cycle}} = \frac{(\text{mults/s})/\#\text{multipliers}}{f}, \quad (11)$$

where mults/s above is measured by taking the number of multiplications required to carry out an execution using conventional algebra and dividing it by the measured execution time, #multipliers is the number of instantiated multipliers in the design, and f is the clock frequency that the hardware design is operating at.

The throughput metric in (11) measures the number of w -bit multiplications being performed, where w is the algorithm input bitwidths. However, in order to execute KMM in hardware, the algorithm input bitwidths w must be larger than the multiplier bitwidths, and the number of larger w -bit multiplications that can be performed per multiplier will be lower than the actual effective number of multiplications being performed per multiplier. Therefore, the maximum achievable value for the metric from (11) will vary depending on the input bitwidths w and is not ideal for reflecting the true amount of computational work being performed per multiplier regardless of the input widths.

To address this, we can instead measure (11) directly in terms of effective m -bit multiplications being performed per multiplier, where m may be smaller than the algorithm input bitwidths w . This derives the following metric for measuring the true amount of effective multiplications being performed per multiplier regardless of the algorithm input bitwidths w :

$$\frac{m\text{-bit mults/multiplier}}{\text{clock cycle}} = \frac{(m\text{-bit mults/s})/\#\text{multipliers}}{f}, \quad (12)$$

where m -bit mults/s above is measured by taking the number of m -bit multiplications required to carry out an execution on w -bit inputs using conventional algebra and dividing it by the measured execution time, #multipliers is the number

of instantiated multipliers in the design, and f is the clock frequency that the hardware design is operating at. Conventional algorithms used in prior work to perform larger w -bit multiplications on smaller m -bit multipliers are the SM or MM algorithms (Algorithm 1 and 3). The number of m -bit multiplications required to carry out a larger w -bit multiplication using conventional algebra (i.e. SM or MM) is equal to the number of w -bit multiplication in the execution times 4^r , where r is equal to:

$$r = \lceil \log_2 n \rceil = \lceil \log_2 \lceil w/m \rceil \rceil. \quad (13)$$

The limit (also referred to as the roof) of the metric in (12) when executing the conventional MM algorithm in hardware is then the following since it has no algebraic optimizations for reducing the computational complexity:

$$\text{MM}_n^{[w]} \frac{m\text{-bit mults/multiplier}}{\text{clock cycle}} \text{roof} = 1. \quad (14)$$

In contrast, the KMM algorithm requires only 3^r smaller-bitwidth multiplications to form every w -bit product rather than 4^r as in MM. Therefore, the multiplier compute efficiency can reach the following limit in KMM architectures:

$$\text{KMM}_n^{[w]} \frac{m\text{-bit mults/multiplier}}{\text{clock cycle}} \text{roof} = \left(\frac{4}{3}\right)^r. \quad (15)$$

F. Area Unit (AU) Compute Efficiency

In this subsection, we define a performance-per-area metric in (23) that accounts for the area overhead of registers, adder units, and multipliers all in a single unit of comparison based around the area of a full adder. Using this abstracted method for modelling the circuit area allows for a general complexity analysis that is less biased towards one specific implementation platform or technology.

We first derive the relative area of adders and registers by modeling that the area of a w -bit adder will be approximately equal to the area of w full adders. We then approximate the area of a w -bit flip-flop/register relative to a w -bit adder according to approximate transistor counts of full adders versus D-flip-flops based on several sources. While there are different specific implementations for these components, we use the approximate transistor count trends for the implementations in prior work [19], [20], [21], where a standard CMOS full adder uses 28 transistors [19] and a 1-bit flip-flop consumes 18-21 transistors [20], [21] (which we then approximate as 19.5), to arrive at the general area estimation shown in (16a) and (16b) of 1 flip-flop equalling the area of approximately $19.5/28 = 0.7$ full adders. So long as these area ratios vary within reasonable bounds as found in prior work [19], [20], [21], the conclusions from our results do not change.

We then model the approximate area of a w -bit multiplier circuit based on the area of a w -bit adder. While there are different possible multiplier circuit implementations, the area of multiplier circuits used in practice commonly scale quadratically with the area of a full adder [16], [17], [18], [22]. Furthermore, the KMM architectures are not tied to being implemented using one specific multiplier circuit type. Therefore, in order to provide a more general analysis and insight

catering to a broader range of possible KMM implementations, we approximate the area of a multiplier based on the general trend of equalling the square of the input bitwidths times the area of a full adder as shown in (16c). We then arrive at the following general area approximations:

$$\text{Area}(\text{ADD}^{[w]}) = w \text{ AU} \quad (16a)$$

$$\text{Area}(\text{FF}^{[w]}) = 0.7 w \text{ AU} \quad (16b)$$

$$\text{Area}(\text{MULT}^{[w]}) = w^2 \text{ AU}. \quad (16c)$$

Based on this, we can then derive the AU of each architecture by substituting in the areas from (16) for each of the corresponding hardware components in the architectures. The area of a baseline MM_1 MXU is then as follows:

$$\begin{aligned} \text{Area}(\text{MM}_1^{[w]}) = XY \text{ Area}(\text{MULT}^{[w]} + 3 \text{FF}^{[w]} \\ + \text{ACCUM}^{[2w]}). \end{aligned} \quad (17)$$

Here, the area of an accumulator is based on Algorithm 5 and its implementation in Fig. 6, where the number of accumulator registers and $(2w+w_a)$ -bit accumulation adders in the MXU are reduced by a factor of p . Based on this, by substituting in the areas in (16) for the adders and registers forming the accumulators in Fig. 6, every p accumulators on average then contain the following area:

$$\begin{aligned} p \text{ Area}(\text{ACCUM}^{[2w]}) = (p-1) \text{ Area}(\text{ADD}^{[2w+w_p]}) \\ + \text{Area}(\text{ADD}^{[2w+w_a]} + \text{FF}^{[2w+w_a]}). \end{aligned} \quad (18)$$

In (17) - (18), X and Y are the MXU width and height in number of multipliers, $w_p = \lceil \log_2 p \rceil$, and w_a is the following additional bitwidth added to account for accumulation:

$$w_a = \lceil \log_2 X \rceil. \quad (19)$$

As discussed in Section IV-D, the register requirements in (17) are derived from the fact that each PE in the MM_1 MXU will contain registers for buffering the a and b inputs being multiplied, as well as one additional b buffer for loading the next b tile into the MXU as the current tile is being multiplied.

The area of the KSMM architecture, which is a baseline MM_1 MXU using KSM multipliers rather than conventional multipliers, is then:

$$\begin{aligned} \text{Area}(\text{KSMM}_n^{[w]}) = XY \text{ Area}(\text{KSM}_n^{[w]} + 3 \text{FF}^{[w]} \\ + \text{ACCUM}^{[2w]}), \end{aligned} \quad (20)$$

where:

$$\begin{aligned} \text{Area}(\text{KSM}_n^{[w]}) = \text{Area}(\text{ADD}^{[2w]}) \\ + 2 \text{ Area}(\text{ADD}^{[2\lceil w/2 \rceil + 4]} + \text{ADD}^{[\lceil w/2 \rceil]}) \\ + \text{Area}(\text{KSM}_{n/2}^{[\lceil w/2 \rceil]} + \text{KSM}_{n/2}^{[\lceil w/2 \rceil + 1]}) \\ + \text{Area}(\text{KSM}_{n/2}^{[\lceil w/2 \rceil]}) \end{aligned} \quad (21a)$$

$$\text{Area}(\text{KSM}_1^{[w]}) = \text{Area}(\text{MULT}^{[w]}). \quad (21b)$$

The addition of c_0 on line 14 of Algorithm 2 is not included in this area estimate because it can be performed before line 13 where c_0 will be on w bits and will not overlap with $c_1 \ll$

w . Therefore, this addition can be performed at no cost in hardware by simply concatenating the two terms together.

The area of the KMM architecture is then:

$$\begin{aligned} \text{Area}(\text{KMM}_n^{[w]}) = 2X \text{ Area}(\text{ADD}^{[\lceil w/2 \rceil]}) \\ + 2Y \text{ Area}(\text{ADD}^{[2\lceil w/2 \rceil + 4 + w_a]} + \text{ADD}^{[2w + w_a]}) \\ + \text{Area}(\text{KMM}_{n/2}^{[\lceil w/2 \rceil]} + \text{KMM}_{n/2}^{[\lceil w/2 \rceil + 1]}) \\ + \text{Area}(\text{KMM}_{n/2}^{[\lceil w/2 \rceil]}) \end{aligned} \quad (22a)$$

$$\text{Area}(\text{KMM}_1^{[w]}) = \text{Area}(\text{MM}_1^{[w]}). \quad (22b)$$

Due to the nature of right/left shifting by a constant offset in custom hardware, the shift operations in the KSMM and KMM algorithms do not add additional area in the corresponding architectures.

We can now compare the AU compute efficiency limits of the MM_1 , KSMM, and KMM architectures using:

$$\frac{\text{throughput}/\text{Area Unit}}{\text{clock cycle}} \text{ roof} = \frac{\text{throughput roof}/\text{Area}(\text{ARCH})}{f}, \quad (23)$$

where ARCH represents one of the mentioned architectures. Throughput roofs are equal for fixed-precision MM_1 , KSMM, and KMM architectures with equal X/Y MXU dimensions. Therefore, the value of (23) for each architecture relative to the MM_1 architecture can be found through the inverse of its AU from (17), (20), or (22) relative to the inverse of the MM_1 AU in (17) as plotted later in Fig. 12.

V. RESULTS

A. Evaluation Metrics

In Section V, we compare the KMM architectures against other designs using the multiplier and Area Unit compute efficiency metrics defined in (12) and (23) from Sections IV-E and IV-F, respectively. These are both used to compare an architecture's throughput per area capabilities regardless of the clock frequency.

Additionally, the multiplier compute efficiency also measures the amount of computational work being performed per compute area regardless of the clock frequency or input bitwidths. This is an important quality because prior works using the same compute platform as us for evaluation only evaluate throughput for input bitwidths w that are equal to the multiplier bitwidths m . However, in order to execute KMM in hardware, the input bitwidths w must be larger than the multiplier bitwidths. Therefore, to fairly compare the performance of the prior works against our KMM architecture, we need to use a performance metric with a maximum achievable value that does not change regardless of the input bitwidths w being executed, which is not the case for the GOPS metric. Furthermore, the multiplier compute efficiency is also useful for comparison with prior works because it is measurable using only throughput, number of multipliers, and frequency, which are commonly provided or derivable in prior works.

The Area Unit compute efficiency metric also accounts for the area overhead of registers and adder units and provides a more general abstracted method for modelling the circuit area

that is less biased towards one specific implementation platform or technology. However, it is only useful for comparing architectures which compute on inputs of the same bitwidth, and it is only derivable when knowing not only the number of multipliers used in an architecture, but also the number of adders and registers which is information that is not readily available from prior works, but we can use it to model the efficiencies of the fixed-precision KMM architecture against our baseline designs which we know all of these details about.

B. Comparison to Prior Work

Although the theoretical concepts presented in this work are general and applicable to both custom integrated circuits and FPGA implementations, our example KMM implementations were validated on FPGA, and we therefore compare against state-of-the-art prior works that are also evaluated on FPGA.

As discussed in Section IV-D, we use an ML accelerator system design based on the one from our previous work [6], which has open-source code available [15], to house and evaluate our example KMM and baseline MXU architectures. Full system-level validation of the experimental accelerator as integrated into the system from our previous work [6] has been done on an Arria 10 SoC Development Kit [23] containing the Arria 10 SX 660 device by measuring throughput in real-time. However, this device contains fewer soft logic resources than the Arria 10 GX 1150 used in the prior works we compare against, and we generate compilation results for our design on the same Arria 10 GX 1150 device used in prior works for a more fair and consistent comparison. Throughput values of our designs on the Arria 10 GX 1150 device are then calculated using an accurate throughput estimation model based on our highly deterministic and time-predictable system implementation, which accurately predicts actual throughputs measured on the Arria 10 SX 660 device available to us. Tables I-III show throughputs for ResNet [24] neural network models.

In Table I, the number of multipliers in the work from An et al. [27] is calculated as $\#DSPs \times 2$, where each DSP in the Intel/Altera FPGAs contains two 18-bit multipliers [28]. The works from Liu et al. [25] and Fan et al. [26] in Table I implement a similar method as in the work from Langhammer et al. [29] to pack two 8-bit multiplications onto each 18-bit multiplier in the DSPs at the cost of additional ALMs and registers, and therefore $\#multipliers = \#DSP \times 4$ in those works. Our architectures in Table I contains $64 \times 64 + 64$ multipliers, where 64×64 multipliers are used in the MXU, while the remaining 64 are located outside the MXU in the Post-GEMM Unit [6] for performing inter-layer quantization rescaling functions. This is also how the number of multipliers is calculated in the architectures in Table II, except there the MXUs contain $64 \times 32 + 32$ multipliers due to using the FFIP method [6]. For the multipliers located in the MXU of our designs in Tables I-II, we also implement a similar method as in the work from Langhammer et al. [29] to pack two smaller-bit multiplications onto each 18-bit multiplier in the DSPs. However, we leave one FFIP+KMM design in Table II without this optimization for a more fair comparison to the FFIP design in our prior work [6] that did not implement this optimization.

Table I compares the KMM architecture with state-of-the-art accelerators evaluated on the same FPGA family for the same instantiated multiplier bitwidths and similar neural network models. The proposed KMM architecture is very efficient, achieving the highest throughput and compute efficiency compared to the prior works in Table I. The KMM design here achieves compute efficiencies approaching the KMM_2 limit of 1.33 when executing on bitwidths in the range of 9-14 bits that is derived in (15) and surpasses the limit of 1 in prior works that is derived in (14).

It is also noted that the proposed systolic arrays in Tables I and II that are integrated into a full accelerator system include a number of other components such as memory subsystems and control as described in our prior work [6], and these other system components form the frequency-limiting critical path as opposed to the proposed systolic-array architectures.

Table II shows an example of how KMM can be combined with other algebraic techniques to further increase compute efficiency limits. FFIP [6] provides a way to reduce the number of required multiplications by a factor of 2, by trading half the multiplications for cheap low-bitwidth additions. Because the number of required multiplications is reduced by 2, the limit for the multiplier compute efficiency metric in (15) becomes 2 for FFIP, and $(8/3)^r$ for FFIP+KMM. In Table II, we combine KMM with FFIP [6] by using an FFIP MXU as the base MXU in the KMM architecture instead of a conventional MM_1 MXU to further increase the compute efficiency compared to standalone FFIP. The FFIP+KMM architectures in Table II have additional memory resources instantiated compared to the FFIP-only design in order to support inference on up to 16-bit inputs, and this also adds a penalty in the soft logic resources and clock frequency. However, the multiplier compute efficiency of the FFIP+KMM designs surpass the FFIP limit of 2, and approach the FFIP+ KMM_2 limit of 2.67.

C. Comparison to Baseline Designs

1) *Precision-Scalable Architectures*: Table I includes the resource usage and performance comparison between the proposed KMM and the baseline MM architectures. The multiplier compute efficiency of KMM surpasses that of the baseline MM architecture when executing on bitwidths in the range of 9-14 bits, achieving compute efficiencies approaching the KMM_2 limit of 1.33 that is derived in (15) and surpassing the limit of 1 of the baseline MM architecture and prior works that is derived in (14), validating KMM's ability to increase compute efficiency as expected from our analysis. This is also reflected in the GOPS from Table I, where the KMM architecture achieves a $1.33 \times$ speedup over MM for input bitwidths in the range of 9-14 bits.

For illustration, Fig. 11 plots the limits of the multiplier compute efficiency metric defined in (12) from Section IV-E for the precision-scalable KMM_2 architecture compared to the conventional precision-scalable MM_2 architecture for $X = Y = 64$. As shown, the KMM architecture surpasses the MM architecture's limit of 1 for this metric, extending the limit to 1.33 for bitwidths 9-14 since the KMM_2 algorithm requires only 3 m -bit multiplications for every w -bit product rather than 4 as in the MM_2 algorithm.

TABLE I

PROPOSED PRECISION-SCALABLE KMM AND BASELINE MM SYSTOLIC-ARRAY ARCHITECTURES INTEGRATED INTO A DEEP LEARNING ACCELERATOR SYSTEM COMPARED WITH EACH OTHER AND PRIOR STATE-OF-THE-ART DEEP LEARNING ACCELERATORS ON ARRIA 10 GX 1150 FPGA.

	TNNLS '22 [25]	TCAD '22 [26]	Entropy '22 [27]		MM ₂ ^[w,8] 64×64			KMM ₂ ^[w,8] 64×64				
DSP optimization ¹	Yes	Yes	No		Yes			Yes				
DSPs	1473	1473	1503		1056			1056				
ALMs	304K	304K	303K		243K			250K				
Registers	889K	890K	-		556K			562K				
Memories	2334	2334	1953		2713			2713				
Frequency (MHz)	200	220	172		320			326				
Model	ResNet-50	VGG16	Bayes ResNet-18	Bayes VGG11	R-CNN (ResNet-50)	R-CNN (VGG16)	ResNet-50	ResNet-101	ResNet-152	ResNet-50	ResNet-101	ResNet-152
Input bitwidth (w)	8	8	8	8	8	8	1-8 / 9-16	1-8 / 9-16	1-8 / 9-16	1-8 / 9-14 / 15-16	1-8 / 9-14 / 15-16	1-8 / 9-14 / 15-16
Throughput (GOPS)	1519	1295	1590	534	719	865	2108 / 527	2304 / 576	2390 / 598	2147 / 716 / 537	2347 / 782 / 587	2435 / 812 / 609
$\frac{8\text{-bit mults/multiplier}}{\text{clock cycle}}$ ²	0.645	0.550	0.639	0.206	0.696	0.837	0.792 / 0.792	0.865 / 0.865	0.898 / 0.898	0.792 / 1.055 / 0.792	0.865 / 1.154 / 0.865	0.898 / 1.197 / 0.898

¹ Determines if the design includes an optimization to pack two smaller-bit multiplications onto the 18-bit multipliers of the DSPs.

² Multiplier compute efficiency, used to compare the amount of computational work being performed per compute area regardless of the input bitwidths or clock frequency, defined in (12) from Section IV-E, relevance explained in Section V-A.

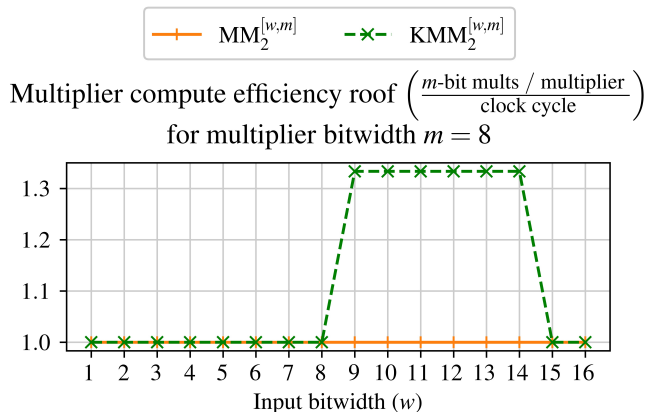


Fig. 11. Maximum achievable multiplier compute efficiencies (derived in Section IV-E) for the precision-scalable MM₂ and KMM₂ architectures.

2) *Fixed-Precision Architectures*: Table III shows synthesis results on a modern Agilinx 7 FPGA device for baseline MM₁, KSMM, and proposed KMM systolic-array architectures in isolation (not integrated into a deep learning accelerator) for different input bitwidths and levels of KSM and KMM recursion. The input bitwidths are intentionally larger than the DSP units' native multiplier bitwidths and are chosen to allow for larger multiplications to be broken down into smaller multiplications of bitwidths at or just below the native widths supported by the DSPs, which house 18-bit multipliers. It is expected that the larger-bit multiplications in the MM₁ designs will be mapped to smaller 16-bit multipliers, and onto fewer 16 to 18-bit multipliers in the KMM and KSMM designs.

The reduction in multiplication complexity of KMM and KSMM achieved through breaking down larger multiplications into smaller-bitwidth multiplications can be seen relative to conventional approaches (evaluated through the MM₁ architec-

tures) by comparing the reduction in number of DSP units for the KMM and KSMM designs relative to MM₁. Furthermore, the reduction in addition complexity of KMM relative to KSMM can be seen in the reduction in ALMs in the KMM architectures compared to the KSMM architectures.

The MM₁ and KSMM architectures innately have a lower clock frequency than KMM because it is expected that each multiplication being performed in the PEs require n^2 or $n^{\log_2 3}$ DSP units, respectively, whereas the KMM designs require only 1 DSP unit in each individual KMM systolic-array PE. This leads to a less localized design. In contrast, the KMM design uses multiple independent systolic arrays requiring 1 DSP unit per multiplication to perform a single 16 to 18-bit multiplication, and the DSPs in each systolic array do not require interconnections with the DSPs in other systolic arrays, leading to a more localized design. Due to this, we provide results of two design variants for each of the MM₁ and KSMM architectures, where one variant contains additional pipelining registers added into the PE datapaths such that the clock frequency can reach closer to that of the KMM designs. However, it can be seen that the MM₁ and KSMM designs are still unable to match the frequency of KMM even with extra pipelining registers, especially for the 64-bit input designs.

In summary, the trend in Table III is that the KMM designs may contain more register resources than the MM₁ and KSMM designs depending on the amount of pipelining registers used, however, the KMM designs use significantly fewer ALM resource than the KSMM designs, significantly fewer DSP units than the MM₁ designs, and achieve significantly higher clock frequencies than both KSMM and MM₁.

Fig. 12 also provides a more general modelling of the performance-per-area of the KMM architectures that is less biased towards one specific implementation platform or tech-

TABLE II
COMPARISON OF AN FFIP [6] SYSTOLIC ARRAY, WHICH DOUBLES PERFORMANCE PER MAC UNIT, WITH COMBINED FFIP+KMM PRECISION-SCALABLE SYSTOLIC ARRAYS WHEN INTEGRATED INTO DEEP LEARNING ACCELERATOR SYSTEMS ON ARRIA 10 GX 1150 FPGA.

	TC '24 [6] (FFIP 64×64)			FFIP+KMM ₂ ^[w,8] 64×64			FFIP+KMM ₃ ^[w,8] 64×64		
DSP optimization ¹	No			No			Yes		
DSPs	1072			1072			552		
ALMs	118K			133K			205K		
Registers	311K			334K			502K		
Memories	1782			2445			2713		
Frequency (MHz)	388			353			341		
Model	ResNet-50	ResNet-101	ResNet-152	ResNet-50	ResNet-101	ResNet-152	ResNet-50	ResNet-101	ResNet-152
Input bitwidth (w)	8	8	8	1-8 / 9-14 / 15-16	1-8 / 9-14 / 15-16	1-8 / 9-14 / 15-16	1-8 / 9-14 / 15-16	1-8 / 9-14 / 15-16	1-8 / 9-14 / 15-16
Throughput (GOPS)	2529	2752	2838	2325 / 775 / 581	2542 / 847 / 635	2637 / 879 / 659	2246 / 749 / 562	2455 / 818 / 614	2547 / 849 / 637
$\frac{8\text{-bit mults/multiplier}}{\text{clock cycle}}$ ²	1.521	1.655	1.707	1.536 / 2.048 / 1.536	1.679 / 2.239 / 1.679	1.742 / 2.322 / 1.742	1.536 / 2.048 / 1.536	1.679 / 2.239 / 1.679	1.742 / 2.322 / 1.742

¹ Determines if the design includes an optimization to pack two smaller-bit multiplications onto the 18-bit multipliers of the DSPs.

² Multiplier compute efficiency, used to compare the amount of computational work being performed per compute area regardless of the input bitwidths or clock frequency, defined in (12) from Section IV-E, relevance explained in Section V-A.

TABLE III
COMPARISON OF PROPOSED FIXED-PRECISION KMM AND BASELINE MM₁ AND KSMM SYSTOLIC-ARRAY ARCHITECTURES IN ISOLATION (WITHOUT INTEGRATION INTO A DEEP LEARNING ACCELERATOR SYSTEM) ON AGILEX 7 FPGA.

	MM ₁ ^[32] 32×32	MM ₁ ^[32] 32×32	KSMM ₂ ^[32] 32×32	KSMM ₂ ^[32] 32×32	KMM ₂ ^[32] 32×32	MM ₁ ^[64] 32×32	MM ₁ ^[64] 32×32	KSMM ₄ ^[64] 32×32	KSMM ₄ ^[64] 32×32	KMM ₄ ^[64] 32×32
Input bitwidth	32	32	32	32	32	64	64	64	64	64
DSPs	2048	2048	1536	1536	1536	8704	8704	4608	4608	4608
ALMs	64K	69K	138K	147K	68K	240K	266K	554K	557K	212K
Registers	165K	225K	306K	481K	257K	237K	712K	447K	1126K	806K
Frequency (MHz)	450	569	386	537	622	203	341	147	345	552
Throughput roof (GOPS)	922	1165	791	1100	1274	416	698	302	707	1131

All designs in this table consume 0 memory resources and are synthesized for an Agilex 7 AGIA040R39A1E1V device.

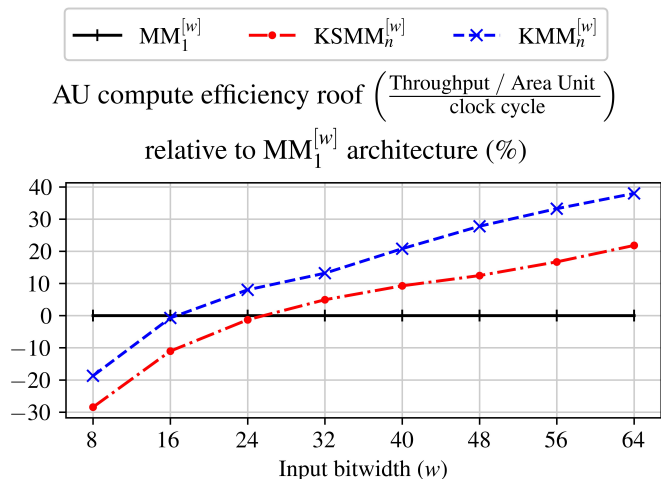


Fig. 12. Maximum achievable AU compute efficiencies (derived in Section IV-F) for the fixed-precision MM₁, KSMM _{n} , and KMM _{n} architectures.

nology by plotting the AU compute efficiency limits derived in Section IV-F that can be achieved for the fixed-precision MM₁, KSMM, and KMM architectures for different supported fixed-precision input widths and instantiated multiplier bitwidths for $X = Y = 64$. The KMM and KSMM architectures for each bitwidth implement as many levels of Karatsuba recursion as possible while still reducing the area, with a minimum of at least one level of Karatsuba recursion being implemented (even if the one level has a larger area than using conventional MM₁). This results in one recursion level being implemented in the KSMM architectures for every bitwidth. For the KMM architectures, this results in one recursion level for bitwidths 8-32, two recursion levels for bitwidths 40-56, and three recursion levels for bitwidth 64.

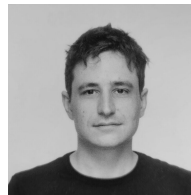
As can be seen, the KMM architecture achieves a higher throughput per Area Unit than the conventional MM₁ architecture starting sooner at a lower bitwidth compared to the KSMM architecture, and it is consistently higher than the KSMM architecture across all input/multiplier bitwidths.

VI. CONCLUSION

In this work, we propose the extension of the scalar Karatsuba multiplication algorithm to matrix multiplication, showing how this maintains the reduction in multiplication complexity of the original Karatsuba algorithm while reducing the complexity of the extra additions. Furthermore, we propose new matrix multiplication hardware architectures for efficiently exploiting the proposed algorithm in custom hardware, showing that they can provide real area or execution time improvements for integer matrix multiplication compared to designs implementing scalar Karatsuba or conventional matrix multiplication algorithms. The proposed architectures are well suited for increasing the efficiency in acceleration of modern workloads that can decompose to large matrix multiplications on integer arithmetic, such as the computationally dominant portion of convolutional neural networks or the attention mechanism of transformer models [30]. We provide a complexity analysis of the algorithm and architectures and evaluate the proposed designs both in isolation and in an end-to-end accelerator system relative to baseline designs and prior state-of-the-art works, showing how they increase the performance-per-area of matrix multiplication hardware.

REFERENCES

- [1] A. Fuchs and D. Wentzlaff, "The accelerator wall: Limits of chip specialization," in *Proc. IEEE Int. Symp. High Perform. Comput. Archit. (HPCA)*, 2019, pp. 1–14.
- [2] X. Liu *et al.*, "WinoCNN: Kernel sharing Winograd systolic array for efficient convolutional neural network acceleration on FPGAs," in *Proc. IEEE 32nd Int. Conf. Appl.-Specific Syst., Arch. Processors (ASAP)*, 2021, pp. 258–265.
- [3] N. P. Jouppi *et al.*, "In-datacenter performance analysis of a tensor processing unit," in *Proc. 44th Annu. Int. Symp. Comput. Archit. (ISCA)*, 2017, pp. 1–12.
- [4] T. Norrie *et al.*, "The design process for Google's training chips: TPUv2 and TPUv3," *IEEE Micro*, vol. 41, no. 2, pp. 56–63, 2021.
- [5] A. Lavin and S. Gray, "Fast algorithms for convolutional neural networks," in *Proc. IEEE Conf. Comput. Vision Pattern Recognit. (CVPR)*, 2016, pp. 4013–4021.
- [6] T. E. Pogue and N. Nicolici, "Fast inner-product algorithms and architectures for deep neural network accelerators," *IEEE Trans. Comput.*, vol. 73, no. 2, pp. 495–509, 2024.
- [7] A. A. Karatsuba and Y. P. Ofman, "Multiplication of many-digit numbers by automatic computers," in *Proc. Doklady Akademii Nauk*, vol. 145, no. 2. Russian Academy of Sciences, 1962, pp. 293–294.
- [8] R. Jain and N. Pandey, "Approximate Karatsuba multiplier for error-resilient applications," *AEU - International Journal of Electronics and Communications*, vol. 130, p. 153579, 2021.
- [9] R. Jain *et al.*, "Booth-encoded Karatsuba: A novel hardware-efficient multiplier," *Advances in Electrical and Electronic Engineering*, vol. 19, no. 3, pp. 272–281, 2021.
- [10] N. Jouppi *et al.*, "TPU v4: An optically reconfigurable supercomputer for machine learning with hardware support for embeddings," in *Proc. 50th Annu. Int. Symp. Comput. Archit. (ISCA)*, 2023, pp. 1–14.
- [11] C. Zhang *et al.*, "Caffeine: Toward uniformed representation and acceleration for deep convolutional neural networks," *IEEE Trans. Comput.-Aided Design Integr. Circuits Syst.*, vol. 38, no. 11, pp. 2072–2085, 2019.
- [12] K. Li *et al.*, "A precision-scalable energy-efficient bit-split-and-combination vector systolic accelerator for NAS-optimized DNNs on edge," in *Proc. Design, Autom. Test Eur. Conf. Exhib. (DATE)*, 2022, pp. 730–735.
- [13] W. Li *et al.*, "Low-complexity precision-scalable multiply-accumulate unit architectures for deep neural network accelerators," *IEEE Trans. Circuits Syst. II, Exp. Briefs*, 2022.
- [14] Y. Umuroglu *et al.*, "Bismo: A scalable bit-serial matrix multiplication overlay for reconfigurable computing," in *Proc. 28th Int. Conf. Field Program. Log. Appl. (FPL)*, 2018, pp. 307–3077.
- [15] T. E. Pogue and N. Nicolici, "FFIP accelerator implementation," 2023. [Online]. Available: <https://github.com/trevorpogue/algebraic-nnhw>
- [16] V. Lakshmi *et al.*, "A novel in-memory wallace tree multiplier architecture using majority logic," *IEEE Trans. Circuits Syst. I*, vol. 69, no. 3, pp. 1148–1158, 2022.
- [17] K. Guo *et al.*, "[DL] a survey of FPGA-based neural network inference accelerators," *ACM Trans. Reconfigurable Technol. Syst.*, vol. 12, no. 1, pp. 1–26, 2019.
- [18] K. Pekmestzi, "Multiplexer-based array multipliers," *IEEE Trans. Comput.*, vol. 48, no. 1, pp. 15–23, 1999.
- [19] F. Moradi *et al.*, "Ultra low power full adder topologies," in *Proc. IEEE Int. Symp. Circuits Syst. (ISCAS)*, 2009, pp. 3158–3161.
- [20] N. Kawai *et al.*, "A fully static topologically-compressed 21-transistor flip-flop with 75% power saving," *IEEE J. Solid-State Circuits*, vol. 49, no. 11, pp. 2526–2533, 2014.
- [21] Y. Cai *et al.*, "Ultra-low power 18-transistor fully static contention-free single-phase clocked flip-flop in 65-nm CMOS," *IEEE J. Solid-State Circuits*, vol. 54, no. 2, pp. 550–559, 2019.
- [22] B. Parhami, *Computer arithmetic: Algorithms and hardware designs*. Oxford University Press, 2010.
- [23] "Intel Arria 10 SoC development kit." [Online]. Available: <https://www.intel.com/content/www/ca/en/products/details/fpga/development-kits/arria10>
- [24] K. He *et al.*, "Deep residual learning for image recognition," in *Proc. IEEE Conf. Comput. Vision Pattern Recognit. (CVPR)*, 2016, pp. 770–778.
- [25] S. Liu *et al.*, "Toward full-stack acceleration of deep convolutional neural networks on FPGAs," *IEEE Trans. Neural Netw. Learn. Syst.*, vol. 33, no. 8, pp. 3974–3987, 2022.
- [26] H. Fan *et al.*, "FPGA-based acceleration for bayesian convolutional neural networks," *IEEE Trans. Comput.-Aided Design Integr. Circuits Syst.*, vol. 41, no. 12, pp. 5343–5356, 2022.
- [27] J. An *et al.*, "An OpenCL-based FPGA accelerator for Faster R-CNN," *Entropy*, vol. 24, no. 10, p. 1346, 2022.
- [28] "Intel Arria 10 native fixed point DSP IP core user guide," 2017. [Online]. Available: <https://www.intel.com/content/www/us/en/docs/programmable/683583/current/intel-arria10-native-fixed-point-dsp-ip-core-user-guide.html>
- [29] M. Langhammer *et al.*, "Extracting INT8 multipliers from INT18 multipliers," in *Proc. IEEE Int. Symp. Field-Programmable Gate Arrays. IEEE*, 2019, pp. 114–120.
- [30] A. Vaswani *et al.*, "Attention is all you need," in *Proc. Annu. Conf. Neural Inf. Process. Syst.*, 2017, pp. 5998–6008.



Trevor E. Pogue Trevor E. Pogue received the B.Eng. degree in Electrical Engineering and the M.A.Sc. degree in Electrical and Computer Engineering from McMaster University, Hamilton, Canada, in 2016 and 2019, respectively. He worked as an intern at Synopsys and AMD in 2018 and 2022–2023, respectively. He is currently a Ph.D. Candidate in the Department of Electrical and Computer Engineering at McMaster University, Hamilton, Canada. His research interests are in the area of hardware acceleration.



Nicola Nicolici (S'99-M'00-SM'11) Nicola Nicolici (S99-M00-SM'11) received the Dipl.Ing. degree in Computer Engineering from the "Politehnica" University of Timisoara, Romania, in 1997 and the Ph.D. degree in Electronics and Computer Science from the University of Southampton, U.K., in 2000. He is currently a Professor with the Department of Electrical and Computer Engineering, McMaster University, Hamilton, Canada. His research interests are in the area of computer-aided design and test. He has authored a number of papers in this area. Dr.

Nicolici was the recipient of the IEEE TTTC Beausang Award for the Best Student Paper at the International Test Conference in 2000 and the Best Paper Award at the IEEE/ACM Design Automation and Test in Europe Conference in 2004.